Biophysical Journal
Article

Biophysical Society

Enthalpy-Entropy Compensation in the Binding of Modulators at Ionotropic Glutamate Receptor GluA2

Christian Krintel,[1] Pierre Francotte,[2] Darryl S. Pickering,[1] Lina Juknaitė,[1] Jacob Pøhlsgaard,[1] Lars Olsen,[1] Karla Frydenvang,[1] Eric Goffin,[2] Bernard Pirotte,[2] and Jette S. Kastrup[1,*]

[1]Department of Drug Design and Pharmacology, Faculty of Health and Medical Sciences, University of Copenhagen, Copenhagen, Denmark; and [2]Department of Medicinal Chemistry, Center for Interdisciplinary Research on Medicines (CIRM), University of Liège, Liège, Belgium

ABSTRACT The 1,2,4-benzothiadiazine 1,1-dioxide type of positive allosteric modulators of the ionotropic glutamate receptor A2 (GluA2) are promising lead compounds for the treatment of cognitive disorders, e.g., Alzheimer's disease. The modulators bind in a cleft formed by the interface of two neighboring ligand binding domains and act by stabilizing the agonist-bound open-channel conformation. The driving forces behind the binding of these modulators can be significantly altered with only minor substitutions to the parent molecules. In this study, we show that changing the 7-fluorine substituent of modulators BPAM97 (**2**) and BPAM344 (**3**) into a hydroxyl group (BPAM557 (**4**) and BPAM521 (**5**), respectively), leads to a more favorable binding enthalpy (ΔH, kcal/mol) from −4.9 (**2**) and −7.5 (**3**) to −6.2 (**4**) and −14.5 (**5**), but also a less favorable binding entropy (−TΔS, kcal/mol) from −2.3 (**2**) and −1.3 (**3**) to −0.5 (**4**) and 4.8 (**5**). Thus, the dissociation constants (K_d, μM) of **4** (11.2) and **5** (0.16) are similar to those of **2** (5.6) and **3** (0.35). Functionally, **4** and **5** potentiated responses of 10 μM L-glutamate at homomeric rat GluA2(Q)$_i$ receptors with EC_{50} values of 67.3 and 2.45 μM, respectively. The binding mode of **5** was examined with x-ray crystallography, showing that the only change compared to that of earlier compounds was the orientation of Ser-497 pointing toward the hydroxyl group of **5**. The favorable enthalpy can be explained by the formation of a hydrogen bond from the side-chain hydroxyl group of Ser-497 to the hydroxyl group of **5**, whereas the unfavorable entropy might be due to desolvation effects combined with a conformational restriction of Ser-497 and **5**. In summary, this study shows a remarkable example of enthalpy-entropy compensation in drug development accompanied with a likely explanation of the underlying structural mechanism.

INTRODUCTION

2-Amino-3-(3-hydroxy-5-methylisoxazol-4-yl)propionic acid (AMPA) receptors mediate most fast excitatory synaptic transmission in the central nervous system (1). They are tetrameric ligand-gated ion channels with each subunit consisting of a flexible intracellular C-terminal domain, a helical transmembrane domain (TMD), an extracellular ligand binding domain (LBD), and an N-terminal domain (2). Although, in the intact receptor, the TMD has fourfold symmetry, the LBDs and N-terminal domains are arranged with twofold symmetry as dimers of dimers. Each LBD consists of the D1 and D2 subdomains with adjacent D1 domains creating a dimeric interface. The receptor is activated by L-glutamate binding in a pocket between the D1 and D2 domains, leading to a conformational change where D2 moves toward D1 (3). This movement creates a conformational strain on the TMD and promotes channel opening. Two mechanisms can lead to channel closure: dissociation of glutamate from the LBD leads to deactivation, whereas rearrangement of the D1:D1 interface with L-glutamate still present in the LBD leads to desensitization (4). Positive allosteric modulators bind in a crevice created by the D1:D1 interface and act by strengthening the agonist-bound state of the receptor attenuating deactivation or by strengthening the interface and thereby slowing desensitization (4,5). Stabilization of the D1:D1 interface can also be accomplished by mutation of a key leucine located at the dimer interface (Leu-483 in the AMPA receptor ionotropic glutamate receptor A2 (GluA2); numbering without signal peptide) to tyrosine, which dramatically slows receptor desensitization (6). Furthermore, this mutation produces a dimeric LBD in solution without altering the modulator binding pocket (4,7).

The modulator BPAM97 (**2**) (Fig. 1) was developed on the basis of the earlier weaker modulators diazoxide and

Submitted December 1, 2015, and accepted for publication April 18, 2016.

*Correspondence: jsk@sund.ku.dk

Christian Krintel and Pierre Francotte contributed equally to this work.

Editor: Axel Brunger.

http://dx.doi.org/10.1016/j.bpj.2016.04.032

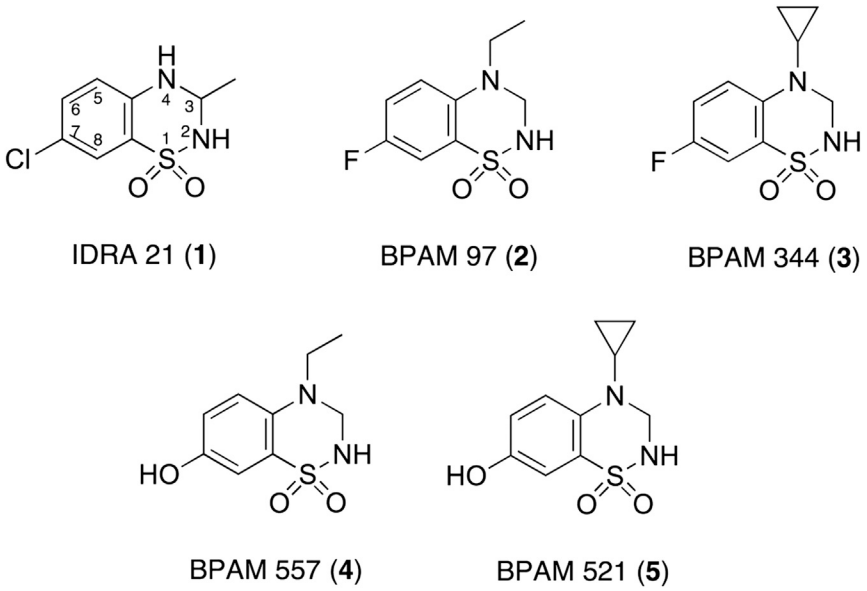

FIGURE 1 Key structures of 1,2,4-benzothiadiazine 1,1-dioxide modulators.

IDRA21 (**1**) (Fig. 1) and showed a 70-fold increase in the binding affinity toward the dimeric LBD construct of ionotropic glutamate receptor A2 (GluA2) (GluA2 LBD-L483Y-N754S) over **1** (7–10). As for **1**, two molecules of **2** bind in the D1:D1 interface where each molecule interacts with Pro-494, Phe-495, Met-496, and Ser-497 across the dimer interface (7,11). Structural analyses suggested that the major reason for the increase in affinity is van der Waals interactions created by the 4-ethyl moiety to Pro-494, Phe-495, and Met-496. This was corroborated by the later development of BPAM344 (**3**) (see Fig. 1, in which the ethyl moiety was altered to a cyclopropyl, further increasing the affinity almost 20-fold to a K_d of 350 nM (12)). Intriguingly, in the structures of both **2** and **3** in complex with GluA2 LBD-L483Y-N754S it was clear that Ser-497 of the receptor adopts two different side-chain conformations of which one interacts with the 7-fluorine of the modulators. In addition, a recent study showed that Ser-497 in GluA2 LBD-L483Y-N754S with BPAM37 bound only adopts a single conformation pointing toward the modulator, despite the lack of a substituent in the 7-position of the modulator (13).

In this study, the 7-fluorine of **2** and **3** was substituted to a hydroxyl group to create the new modulators BPAM557 (**4**) and BPAM521 (**5**), respectively (see Fig. 1). It was hypothesized that the hydroxyl group would form favorable hydrogen bonding to Ser-497. Following synthesis, the two new modulators were characterized using two-electrode voltage clamp (TEVC) electrophysiology, x-ray structure determination, and isothermal titration calorimetry (ITC). We show that the introduction of a hydroxyl group instead of fluorine in the 7-position of the modulator dramatically alters the thermodynamics of binding at GluA2 LBD-L483Y-N754S, while retaining binding affinities similar to those of **2** and **3**.

MATERIALS AND METHODS

Synthesis of the target compounds BPAM557 (4) and BPAM521 (5)

All commercial chemicals and solvents were reagent grade and used without further purification. Melting points were determined on a Stuart SMP3 apparatus (Barloworld Scientific France SAS, Nemours, France) in open capillary tubes and are uncorrected. NMR spectra were recorded on a Bruker Avance 500 spectrometer (^{1}H: 500 MHz; ^{13}C: 125 MHz; Bruker Daltonik, Bremen, Germany) using dimethylsulfoxide-d_6 (DMSO-d_6) as solvent and tetramethylsilane as the internal standard; chemical shifts are reported in δ values (ppm) relative to internal tetramethylsilane. The abbreviations s, singlet; d, doublet; t, triplet; q, quadruplet; m, multiplet; and bs, broad signal are used throughout. Elemental analyses (C, H, N, S) were carried out on a Thermo Flash EA 1112 series elemental analyzer (Thermo Electron, Milan, Italy). All reactions were followed by thin layer chromatography (silica gel 60F_{254}, Merck, Darmstadt, Germany) and visualization was accomplished with ultraviolet light (254 or 366 nm).

*4-Cyclopropyl-7-methoxy-4H-1,2,4-benzothiadiazine 1,1-dioxide (**9**)*

A solution of 2-amino-5-methoxybenzenesulfonamide (**6**) (1.0 g; 4.9 mmol) (14) in methanol (20 ml) was supplemented with (1-ethoxycyclopropyloxy)trimethylsilane (4 ml) and glacial acetic acid (4 ml) and refluxed for 18 h. The reaction mixture was then evaporated to dryness under reduced pressure. The resulting oily residue was treated with water (30 ml) and extracted with chloroform (3 × 30 ml). The organic layers were collected and dried over anhydrous $MgSO_4$. The filtrate was evaporated to dryness and the resulting oily residue, consisting of crude 5-methoxy-2-(1-methoxycyclopropylamino)benzenesulfonamide (**7**) (transacetalization reaction in methanol leading to the methoxy-substituted compound), was used in the next step without further purification.

The solution of **7** in tetrahydrofuran (50 ml) was supplemented with sodium borohydride (2.0 g, 52.9 mmol) and boron trifluoride diethyl etherate (2 ml) and refluxed for 18 h. The solvent was then removed by distillation

under reduced pressure and the residue was treated with water (30 ml). The aqueous suspension was adjusted to pH 4 by means of 6N HCl and then extracted with chloroform (3 × 30 ml). The organic layers were collected and dried over anhydrous $MgSO_4$. The filtrate was concentrated to dryness under reduced pressure and the resulting oily residue, consisting of crude 2-cyclopropylamino-5-methoxybenzenesulfonamide (**8**), was used in the next step without further purification.

The mixture of **8** in triethyl orthoformate (10 ml) was heated in an open vessel at 150°C for 6 h. The resulting suspension was cooled on an ice bath and the insoluble material was collected by filtration, washed with diethyl ether, and dried. The solid was dissolved in a hot mixture of acetone and methanol and the solution was treated with charcoal, filtered, and concentrated to dryness. The residue of the title compound (**9**) was purified by crystallization in methanol (overall yields: 20–30%). White solid: mp 216–219°C; ^{1}H NMR (DMSO-d_6) δ 1.00 (m, 2H, CH(CH_2)$_2$), 1.15 (m, 2H, CH(CH_2)$_2$), 3.37 (m, 1H, CH(CH$_2$)$_2$), 3.87 (s, 3H, OCH_3), 7.30 (d, J = 2.9 Hz, 1H, 8-*H*), 7.41 (dd, J = 9.3 Hz/2.9 Hz, 1H, 6-*H*), 7.80 (d, J = 9.3 Hz, 1H, 5-*H*), 8.07 (s, 1H, 3-*H*). ^{13}C NMR (DMSO-d_6) δ 7.2 (CH(*C*H$_2$)$_2$), 32.1 (*C*H(CH$_2$)$_2$), 56.0 (O*C*H$_3$), 106.0 (C-8), 118.9 (C-5), 121.0 (C-6), 123.2 (C-8a), 130.1 (C-4a), 150.6 (C-3), 157.7 (C-7).

*4-Cyclopropyl-3,4-dihydro-7-methoxy-2H-1,2,4-benzothiadiazine 1,1-dioxide (**10**)*

The solution of 4-cyclopropyl-7-methoxy-4*H*-1,2,4-benzothiadiazine 1,1-dioxide (**9**) (0.2 g, 0.79 mmol) in isopropanol (5 ml) was supplemented with finely divided sodium borohydride (0.1 g, 2.64 mmol) and the mixture was heated at 50°C for 5–10 min. The solvent was removed by distillation under reduced pressure and the residue was treated with water (10 ml) and adjusted to pH 4 by means of 6N HCl. The suspension was extracted with methylene chloride (3 × 15 ml). The organic layers were dried over $MgSO_4$ and filtered. The filtrate was evaporated to dryness and the solid residue of the crude compound **10** was crystallized in methanol/water 1:1 (yields: 70–80%). White solid: mp 154–156°C; ^{1}H NMR (DMSO-d_6) δ 0.62 (m, 2H, CH(CH_2)$_2$), 0.87 (m, 2H, CH(CH_2)$_2$), 2.42 (m, 1H, CH(CH$_2$)$_2$), 3.73 (s, 3H, OCH_3), 4.59 (s, 2H, 3-CH_2), 7.04 (d, J = 3.0 Hz, 1H, 8-*H*), 7.12 (dd, J = 9.2 Hz/3.0 Hz, 1H, 6-*H*), 7.27 (d, J = 9.2 Hz, 1H, 5-*H*), 7.89 (s, 1H, N*H*). ^{13}C NMR (DMSO-d_6) δ 8.3 (CH(*C*H$_2$)$_2$), 29.8 (*C*H(CH$_2$)$_2$), 55.7 (O*C*H$_3$), 61.2 (C-3), 107.4 (C-8), 116.5 (C-5), 120.7 (C-6), 123.5 (C-8a), 138.6 (C-4a), 151.1 (C-7). Anal. ($C_{11}H_{14}N_2O_3S$) theoretical: C, 51.95; H, 5.55; N, 11.02; S, 12.61. Found: C, 51.76; H, 5.54; N, 10.83; S, 12.39.

*4-Cyclopropyl-3,4-dihydro-7-hydroxy-2H-1,2,4-benzothiadiazine 1,1-dioxide (**5**)*

The solution of 4-cyclopropyl-3,4-dihydro-7-methoxy-2*H*-1,2,4-benzothiadiazine 1,1-dioxide (**10**) (0.1 g, 0.39 mmol) in chloroform (6 ml) was cooled on an ice bath and then supplemented with boron tribromide (0.3 ml). After 20 h stirring, the reaction mixture was carefully poured on water (10 ml) and the organic solvent was removed by distillation under reduced pressure. The aqueous layer was extracted with ethyl acetate (3 × 40 ml). The collected organic layers were dried over $MgSO_4$ and filtered. The filtrate was evaporated to dryness and the residue was dissolved in ethyl acetate (2 ml). The addition of hexane (10 ml) gave rise to the precipitation of the title compound, which was collected by filtration, washed with hexane, and dried (yields: 80%). White solid: mp 187–189°C; ^{1}H NMR (DMSO-d_6) δ 0.60 (m, 2H, CH(CH_2)$_2$), 0.84 (m, 2H, CH(CH_2)$_2$), 2.37 (m, 1H, CH(CH$_2$)$_2$), 4.54 (s, 2H, 3-CH_2), 6.91 (d, J = 2.7 Hz, 1H, 8-*H*), 6.93 (dd, J = 8.9 Hz/2.9 Hz, 1H, 6-*H*), 7.18 (d, J = 8.9 Hz, 1H, 5-*H*), 7.83 (bs, 1H, N*H*), 9.34 (bs, 1H, O*H*). ^{13}C NMR (DMSO-d_6) δ 8.2 (CH(*C*H$_2$)$_2$), 29.9 (*C*H(CH$_2$)$_2$), 61.3 (C-3), 109.2 (C-8), 116.5 (C-5), 121.1 (C-6), 123.8 (C-8a), 137.3 (C-4a), 149.1 (C-7). Anal. ($C_{10}H_{12}N_2O_3S$) theoretical: C, 49.99; H, 5.03; N, 11.66; S, 13.34. Found: C, 49.83; H, 5.07; N, 11.69; S, 13.02.

*3,4-Dihydro-4-ethyl-7-hydroxy-2H-1,2,4-benzothiadiazine 1,1-dioxide (**4**)*

The title compound was prepared as described for **5** starting from 3,4-dihydro-4-ethyl-7-methoxy-2*H*-1,2,4-benzothiadiazine 1,1-dioxide obtained as previously described (8). White solid: mp 201–203°C; ^{1}H NMR (DMSO-d_6) δ 1.06 (t, J = 7 Hz, 3H, CH$_2$CH_3), 3.36 (m, 2H, CH_2CH$_3$), 4.57 (s, 2H, 3-CH_2), 6.80 (d, J = 8.8 Hz, 1H, 5-*H*), 6.88-6.91 (m, 2H, 6-*H*/8-*H*), 7.85 (bs, 1H, N*H*), 9.25 (bs, 1H, O*H*). ^{13}C NMR (DMSO-d_6) δ 11.8 (CH$_2$*C*H$_3$), 43.7 (*C*H$_2$CH$_3$), 60.4 (C-3), 109.3 (C-8), 116.2 (C-5), 121.6 (C-6), 123.5 (C-8a), 136.1 (C-4a), 148.1 (C-7). Anal. ($C_9H_{12}N_2O_3S$) theoretical: C, 47.35; H, 5.30; N, 12.27; S, 14.04. Found: C, 47.45; H, 5.33; N, 12.34; S, 13.72.

Pharmacology

TEVC functional responses

Recombinant rat GluA2(Q)$_i$ cRNA was transcribed in vitro (AmpliCap-Max T7, Cellscript, Madison, WI) and microinjected into *Xenopus lævis* oocytes. Oocytes were used for TEVC recordings 2–5 days postinjection. Recordings were made at room temperature at holding potentials in the range of −15 to −70 mV, where the oocytes were continuously superfused with Ca^{2+}-free frog Ringer's solution (115 mM NaCl, 2 mM KCl, 1.8 mM $BaCl_2$, 5 mM HEPES, pH 7.6). Potentiating compounds were prepared in Ca^{2+}-free frog Ringer's solution containing 10 μM L-glutamate. DMSO was used to dissolve **4**, which was then diluted in Ringer's/Glu solution to 0.2% (v/v) DMSO at 1 mM compound. Compounds were applied stepwise by bath application for 30–60 s until a plateau response was obtained at each concentration. Data were fit to a logistic equation to determine the EC_{50} and n_H using GraphPad Prism v6 (GraphPad Software, San Diego, CA).

Expression, purification, and x-ray structure determination

Protein expression, purification, and cocrystallization

The rat GluA2 LBD-L483Y-N754S protein was expressed and purified as previously described (7). Cocrystals with **5** were obtained by the hanging drop vapor diffusion technique at 7°C. The drops consisted of 1 μl of protein solution and 1 μl of reservoir solution. The protein solution contained 5.7 mg/ml GluA2 LBD-L483Y-N754S in 10 mM Hepes, 20 mM NaCl, 1 mM EDTA, and 5 mM L-glutamate. For cocrystallization experiments 0.5 mg of **5** was added to 150 μl of protein solution and the mixture was incubated for 24 h before crystallization. Crystallization conditions were 20% PEG4000, 0.3 M lithium sulfate, and 0.1 M phosphate-citrate, pH 4.5. Crystals were briefly transferred to reservoir buffer containing 20% glycerol and then flash cooled in liquid nitrogen.

Data collection and structure determination

Diffraction data were collected at beamline I911-3 at MAX-lab (Lund, Sweden) (15). The data were processed using iMosflm and Scala (16,17) and the structure solved by molecular replacement using Phaser (18) with the structure of GluA2 LBD-L483Y-N754S with **2** (Protein Data Bank (PDB): 3TDJ, molA) as the search model (7). Further model building was done in Coot (19) and refinements were performed using Phenix (20). Topology and parameter files for ligands were obtained using the Schrödinger software (Maestro, version 9.1; Schrödinger, LLC, New York, NY). D1-D2 domain closures were calculated relative to the apo structure (PDB: 1FTO, molA) (3), using DynDom (21). Three-dimensional-structure figures were prepared using The PyMOL Molecular Graphics System (version 1.7.2.3, Schrödinger, LLC).

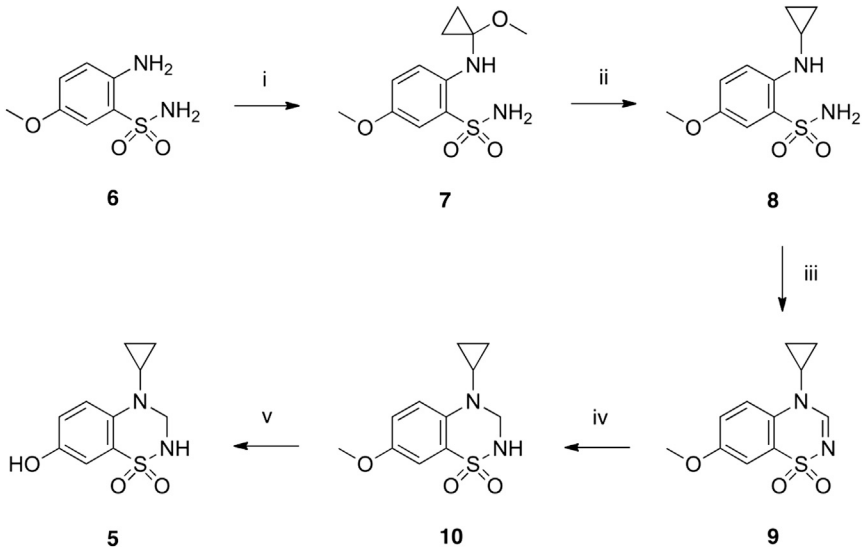

FIGURE 2 Synthesis of compounds. Reagents: i, (1-ethoxycyclopropyloxy)trimethylsilane, HOAc, MeOH; ii, $NaBH_4$, $BF_3.Et_2O$, THF; iii, $HC(OEt)_3$; iv, $NaBH_4$, isopropanol; v, BBr_3, $CHCl_3$. Compound **5** corresponds to BPAM521.

ITC

ITC was performed at 25°C using an ITC200 microcalorimeter (GE Healthcare) with a cell volume of 200 μl for **4** and a VP-ITC microcalorimeter (GE Healthcare) with a cell volume of 1.4 ml for **5**. Before the experiments, the protein was dialyzed twice against 100 mM Hepes, 100 mM NaCl, 2 mM KCl, and 5 mM L-glutamate, pH 7.0 and ligands were dissolved in the same buffer. For measurement of **4** binding, the dimeric protein concentration was 45 μM and a concentration of 1.5 mM of **4** was used for titration. For measurement of **5** binding, the dimeric protein concentration was 30 μM and a concentration of 0.6 mM of **5** was used for titration. For **4**, the experiments were performed as 20 injections with 3-min intervals, using 0.4 μl in the first injection and 2 μl in the following injections. For **5**, the experiments were performed as 20 injections with 3-min intervals, using 2 μl in the first injection and 15 μl in the following injections. Data analysis was performed with the Origin 7.0 software (OriginLab, Northampton, MA) using a single binding site model. The first data point was discarded. The reported ΔH, $-T\Delta S$, and K_d are mean values of three experiments. The protein concentration was determined by ultraviolet absorption.

Calculation of solvation energy

Structures of **2**–**5** were optimized in the gas phase with B3LYP/6-31G** and the solvation energies determined with a single point calculation using the SM8 solvation model (22). The calculations were carried out with Jaguar (Jaguar, version 8.8, Schrödinger, LLC, 2015).

RESULTS AND DISCUSSION

Synthesis and functional characterization of BPAM557 (4) and BPAM521 (5)

The synthetic pathway to the 7-hydroxy-substituted 3,4-dihydro-2*H*-1,2,4-benzothiadiazine 1,1-dioxide BPAM521 (**5**) is illustrated in Fig. 2. Starting from 2-amino-5-methoxybenzenesulfonamide (**6**) obtained as previously described (14) the introduction of a cyclopropyl group on the amine function of **6** was achieved by using (1-ethoxycyclopropyloxy)trimethylsilane to form the hemiaminal ether intermediate **7**. A transacetalization reaction in methanol occurred leading to the methoxy-substituted compound **7** instead of its ethoxy-substituted counterpart. Compound **7** further reacted with boron trifluoride diethyl etherate to provide the key intermediate **8**, which was engaged in the ring closure reaction with triethyl orthoformate to form the 4*H*-1,2,4-benzothiadiazine 1,1-dioxide **9**. Saturation of the double bond at the 2,3-positions of **9** was performed by the reaction of the latter with sodium borohydride in isopropanol giving rise to the 3,4-dihydro-2*H*-1,2,4-benzothiadiazine 1,1-dioxide **10**. The methoxy group at the 7-position of **10** was converted into the hydroxy group after its reaction with boron tribromide in chloroform, leading to the final target compound **5**. To

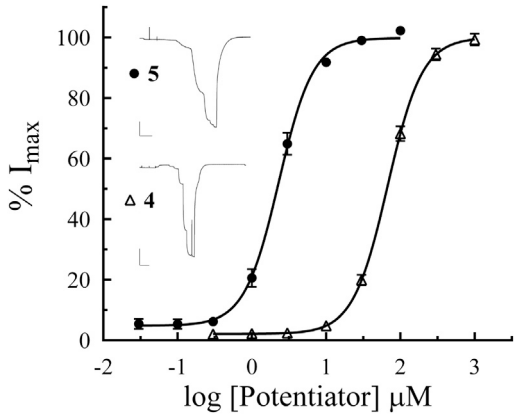

FIGURE 3 Potentiation of 10 μM L-glutamate responses by BPAM557 (**4**) and BPAM521 (**5**) at homomeric rat GluA2(Q)$_i$ expressed in *X. lævis* oocytes and recorded by TEVC. Shown are mean ± SE of pooled data from 7 to 8 experiments normalized to the maximum current response of each oocyte. Insets: sample traces from representative experiments for **4** ($V_h = -20$ mV) and **5** ($V_h = -25$ mV). The scale bars = 200 nA and 1 min.

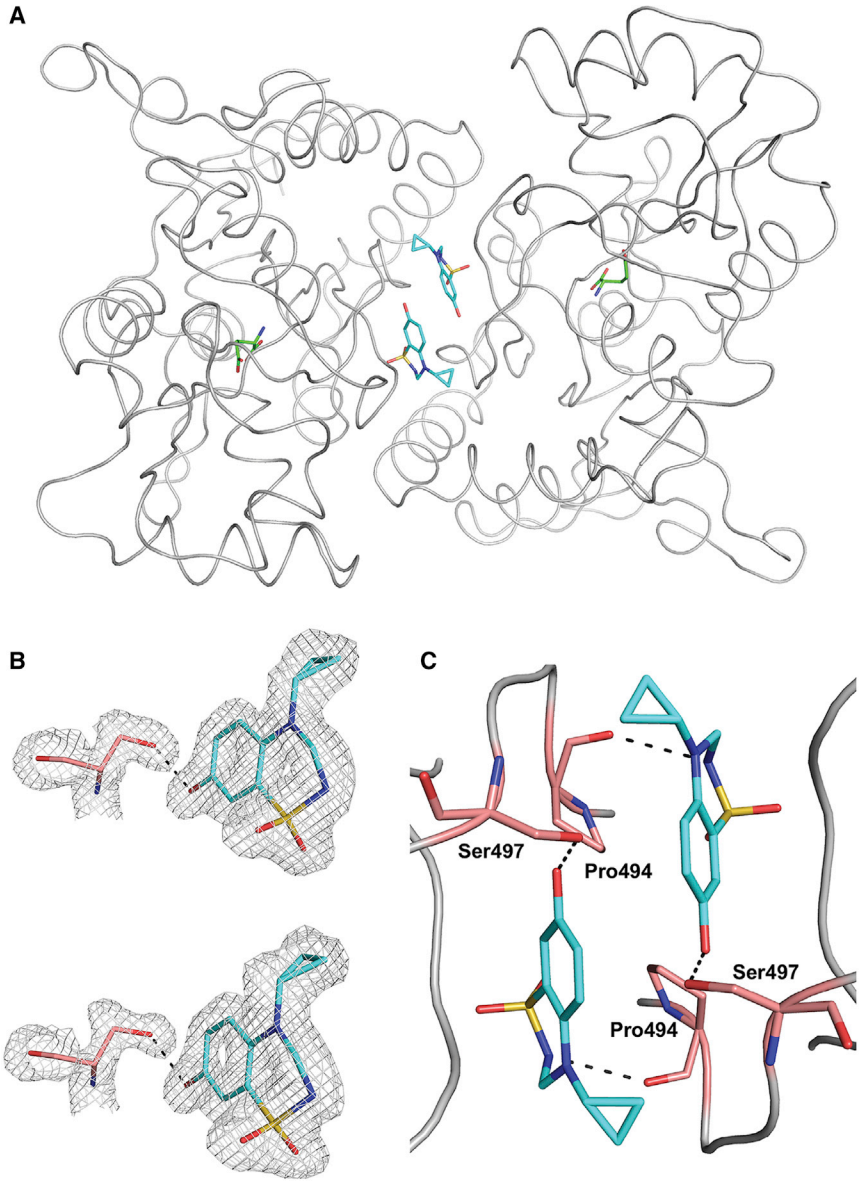

FIGURE 4 Structure of GluA2 LBD in complex with the neurotransmitter L-glutamate and the positive allosteric modulator BPAM521 (**5**). (*A*) Position of **5** (*cyan* at dimer interface) and L-glutamate (*green* in the middle of the GluA2 LBD) in the GluA2 LBD-L483Y-N754S dimer (*gray*). (*B*) Ser-497 of molA (*upper*) and molB (*lower*) shown with the interacting modulator molecule. A simulated annealing 2 F_o-F_c OMIT map carved at 1.5 Å is shown at sigma level 1. (*C*) Possible polar contacts to Pro-494 and Ser-497 (*salmon* in sticks presentation) are indicated by black dashed lines. To see this figure in color, go online.

prepare compound BPAM557 (**4**) (the 4-ethyl-substituted analog of **5**), the previously described 3,4-dihydro-4-ethyl-7-methoxy-2*H*-1,2,4-benzothiadiazine 1,1-dioxide **17** (the 4-ethyl-substituted analog of **10**) (8) was treated with boron tribromide according to the experimental conditions applied to compound **10**.

The synthesized compounds **4** and **5** were evaluated as AMPA receptor potentiators in a voltage clamp assay (TEVC) on *Xenopus* oocytes expressing recombinant rat GluA2(Q)$_i$. In the potentiation of 10 μM L-glutamate responses, **5** was the more potent compound (mean ± SE) EC_{50} = 2.45 ± 0.23 μM (n = 8), whereas **4** was 27-fold less potent, EC_{50} = 67.3 ± 5.1 μM (n = 7). Both compounds exhibited steep concentration-response curves (Fig. 3) with Hill slopes near 2 (**5**, n_H = 2.15 ± 0.25; **4**, n_H = 1.90 ± 0.03). Thus, the Hill slope indicates two pairs of binding sites, which is in agreement with recent studies showing a second modulator binding site to produce both an increase in positive cooperativity and a decrease in the EC_{50} for dimerization (23).

Structure determination of GluA2 LBD-L483Y-N754S in complex with BPAM521 (5)

The purpose of cocrystallizing BPAM521 (**5**) with the GluA2 LBD was to investigate the impact of exchanging the fluorine atom in the previously published modulator BPAM344 (**3**) with a hydroxyl group on the binding mode and in particular on the orientation of Ser-497.

GluA2 LBD-L483Y-N754S in complex with L-glutamate and **5** crystallized as a dimer (Fig. 4 *A*; Table 1) identical to other glutamate bound GluA2 LBD structures. This mutant

TABLE 1 X-Ray Data Collection and Refinement Statistics of GluA2-LBD-L483Y-N754S in Complex with L-glutamate and BPAM521 (5)

	Data Collection
Space group	$P2_12_12$
a, b, c (Å)	98.79, 122.48, 47.54
Resolution (Å)	34.25–6.07 (2.02–1.97)[a]
Redundancy	5.1 (5.1)
Completeness (%)	99.9 (99.9)
R_{merge} (%)[b]	8.8 (26.0)
I/sigmaI	5.2 (1.9)
Refinement	
R_{work}/R_{free} (%)[c]	16.2/21.0
No. of nonhydrogen atoms	4836
No. of residues (molA/B)	263/263
No. of L-glutamate/BPAM521(**5**)/water/glycerol/acetate/chloride/sulfate/PEG	2/2/444/4/9/3/4/2
RMS Deviations	
Bond lengths (Å)	0.007
Bond angles (deg)	1.0
No. residues in allowed areas of Ramachandran plot (%)[d]	100
Average B Values (Å^2)	
molA/B	18.5/14.3
L-glutamate/BPAM521(5)/water/glycerol/acetate/chloride/sulfate/PEG	9.9/4.5/24.9/39.0/41.2/50.5/41.2/43.4

[a]Values for the outermost resolution shell are denoted in parentheses.
[b]$R_{merge} = \Sigma_{hkl}\Sigma_i|I_i(hkl) - I(hkl)|/\Sigma_{hkl}\Sigma_i|I_i(hkl)|$, with Miller indices hkl, the intensity of an individual measurement of the reflection ($I_i(hkl)$), and the intensity from multiple observations ($I_{(hkl)}$).
[c]$R_{work} = \Sigma_{hkl}|F_o - F_c|/\Sigma_{hkl}|F_o|$, with observed ($|F_o|$) and calculated ($|F_c|$) structure factor amplitudes. R_{free} is calculated with 5% reflections omitted from the refinement process.
[d]PROCHECK (26) was used to calculate the Ramachandran plot.

construct was used as it has previously been shown to form a dimer in solution without altering the modulatory site (7). Two molecules of **5** could be unambiguously fitted into electron densities found at the dimeric interface between the two D1 neighboring subdomains (Fig. 4 *B*). The D1-D2 domain closure was found to be 20.5° (molA) and 19.2° (molB), which is similar to other structures with L-glutamate (3).

The modulator molecules adopt a binding mode almost identical to the one seen for the previously published compound **3** (12). As with **3**, the N4 cyclopropyl moiety of **5** makes nonpolar contacts with backbone atoms of Phe-495 and Met-496 and a hydrogen bond is formed between the N2 secondary amide of **5** and the carbonyl oxygen of Pro-494 (Fig. 4 *C*). The most important difference between these two structures is the orientation of Ser-497. In the complex with **3** the side chain of Ser-497 adopts two different conformations, one pointing toward and one away from **3**. However, in the GluA2 LBD structure with **5** the side chain of Ser-497 is seen predominantly in the conformation pointing toward **5** (Fig. 4, *B* and *C*). The conformation of Ser-497 pointing away from **5** was refined to occupancy of 0.13 (molA) and 0.17 (molB) and was therefore not included in the structure. This allows the formation of a hydrogen bond between the

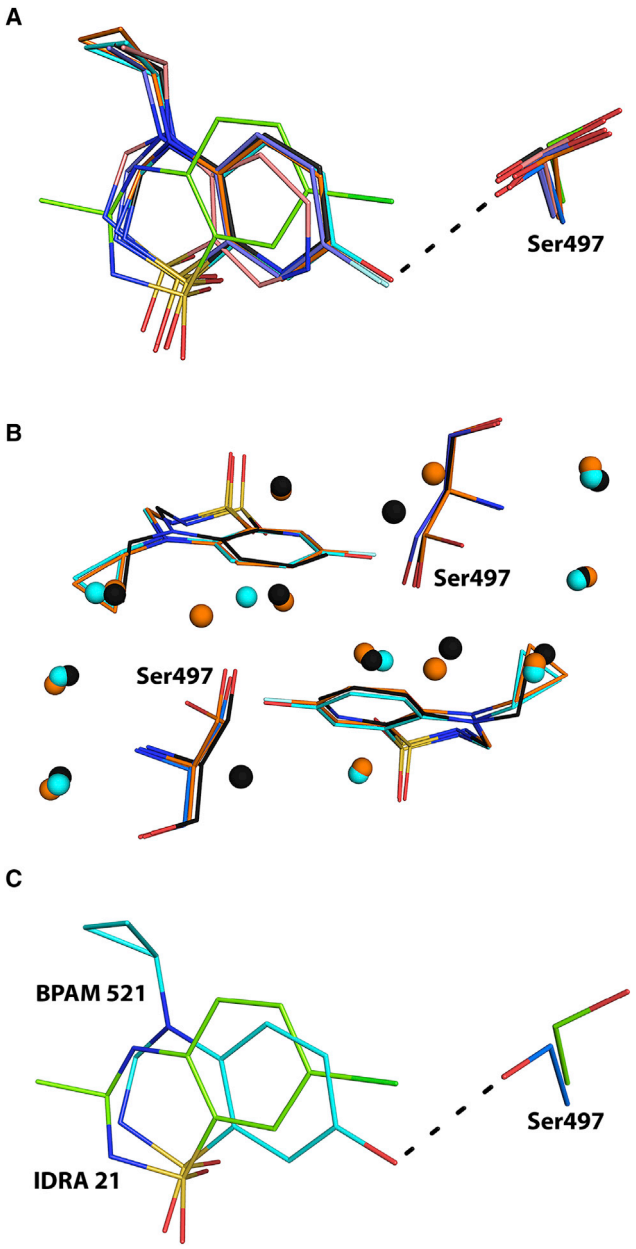

FIGURE 5 Comparison of GluA2 LBD structures with modulators. (*A*) Conformations of Ser-497 in GluA2 with different modulators. An overlay of the D1 subdomains of the GluA2 LBD in complex with BPAM521 (**5**; *cyan*), BPAM97 (**2**; *magenta*; PDB: 3TDJ), BPAM344 (**3**; *orange*; PDB: 4N07), BPAM37 (**12**; *dark gray*; PDB: 4U4X), BPAM25 (**11**; *salmon*; PDB: 4U4S), and IDRA21 (**1**; *green*; PDB: 3IL1). Modulators and the corresponding Ser-497 are shown in stick representation. (*B*) Overlay of the D1 subdomains of GluA2 LBD in complex with **5**, **3**, and **12** (*black*). Modulators and their corresponding Ser-497 are shown in stick representation. Water molecules at a distance up to 4.0 Å of the Ser-497 hydroxyl group in both conformations and the hydroxyl group of **5** are shown as spheres. (*C*) Overlay of GluA2 LBD structures with **1** and **5**. Only the two modulators and Ser-497 are shown. To see this figure in color, go online.

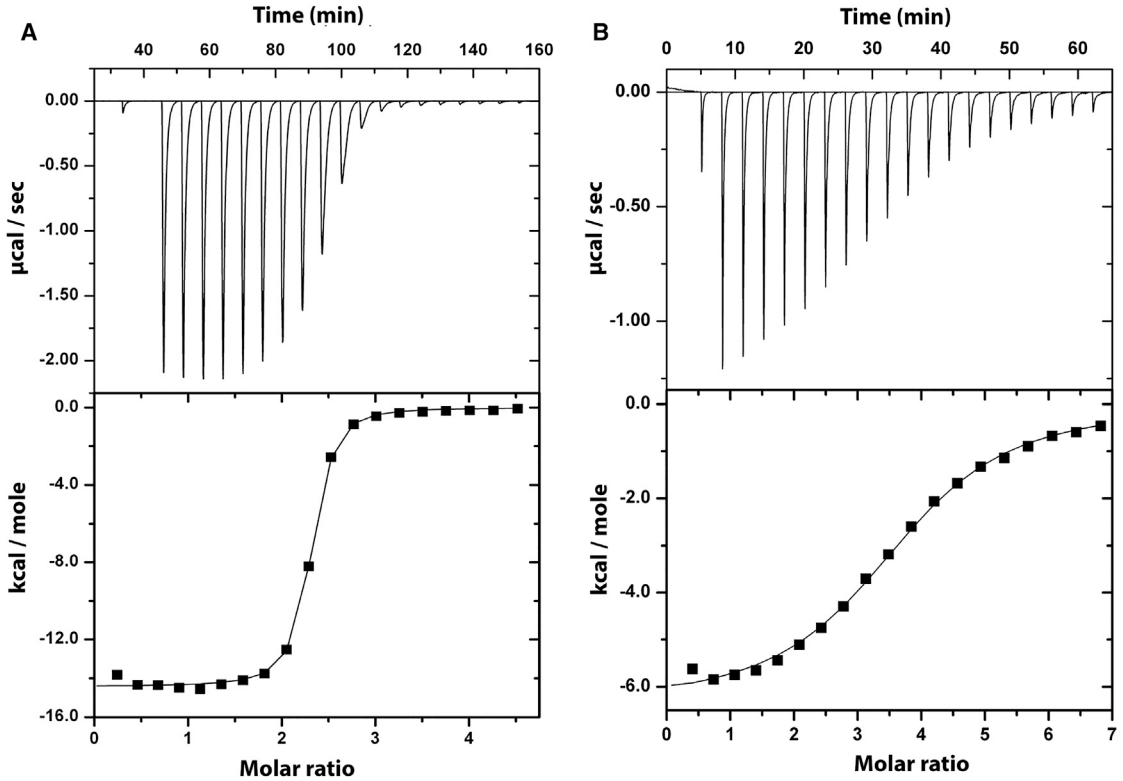

FIGURE 6 ITC studies of BPAM521 (**5**) and BPAM557 (**4**) binding to the GluA2 LBD-L483Y-N754S. Raw data (*top panels*) and isotherms (*bottom panels*) are presented. The graphs show that heat is developed after each injection and that the signal is diminished when the protein becomes saturated with ligand. (*A*) Titration of **5** into GluA2 LBD-L483Y-N754S. (*B*) Titration of **4** into GluA2 LBD-L483Y-N754S.

hydroxyl group of **5** and the hydroxyl group of Ser-497. Of all available structures of GluA2 LBD in complex with 1,2,4-benzothiadiazine 1,1-dioxides it is only in the complexes with **5** and BPAM37 (**12**) (see Fig. 7) that Ser-497 adopts this single conformation pointing toward the modulator (Fig. 5 *A*). This conformation of Ser-497 is also the predominant conformation seen when glutamate and no modulator is bound (GluA2 flop: PDB: 1FTJ and 3DP6; GluA2 flip: 2UXA). Despite different conformations of Ser-497 in GluA2 upon binding of either **12** or **5** versus **3**, a similar network of solvent molecules are present in the modulator binding pocket in all three structures (Fig. 5 *B*). Interestingly, in this context compound **12** is very different from **5** by lacking a 7-position substituent and it is therefore not able to directly interact with Ser-497. Therefore, the observation that the orientation of Ser-497 is the same in the complex with **12** as well as in structures void of modulators, suggests that this orientation of Ser-497 is likely to be due to lack of repulsion by the modulator.

Thermodynamics of binding using isothermal titration calorimetry

The major difference in binding mode of BPAM521 (**5**) and BPAM344 (**3**) in GluA2 LBD is the formation of a hydrogen bond from the hydroxyl group in **5** to the side-chain hydroxyl group of Ser-497. Polar contacts are likely to be reflected in enthalpic contributions to binding energies and we therefore measured the thermodynamics of binding using ITC (Fig. 6). The GluA2 LBD-L483Y-N754S was used for studying modulator binding to GluA2 as it is dimeric in solution and presents a preformed modulator binding pocket, thereby isolating the event of modulator binding from that of dimerization (7). Even though the binding affinity of **5** ($K_d = 0.16\ \mu M$) was found to be similar to that of **3** ($K_d = 0.35\ \mu M$ (12)), dramatically altered enthalpic and entropic contributions to the binding energy were seen (Table 2). Compared to **3**, the new modulator **5** provides a strong gain in binding enthalpy (**5**: $\Delta H = -14.5$ kcal/mol, **3**: $\Delta H = -7.5$ kcal/mol (12)), but also an equally strong unfavorable entropy compensation (**5**: $-T\Delta S = 4.8$ kcal/mol, **3**: $-T\Delta S = -1.3$ kcal/mol (12)). This pattern was found to be the same for BPAM557 (**4**) ($K_d = 11.2\ \mu M$, $\Delta H = -6.2$ kcal/mol, $-T\Delta S = -0.5$ kcal/mol) and the related compound BPAM97 (**2**) ($K_d = 5.6\ \mu M$, $\Delta H = -4.9$ kcal/mol, $-T\Delta S = -2.3$ kcal/mol) (7). This shows that introduction of the 7-hydroxyl group alters the thermodynamics so that binding of **4** and **5** is mainly driven by enthalpy.

An overview of the thermodynamic contributions to the binding energy of all BPAMs reported to date is shown in

TABLE 2 Isothermal Titration Calorimetry Using GluA2 LBD-L483Y-N754S

Compound	K_d (μM)	ΔH (kcal/mol)	−TΔS (kcal/mol)	N[a]
BPAM521 (**5**)	0.16 ± 0.01[b]	−14.5 ± 0.2	4.8 ± 0.2	2.2 ± 0.03
BPAM344 (**3**)[c]	0.35 ± 0.02	−7.5 ± 0.2	−1.3 ± 0.2	2.7 ± 0.1
BPAM557 (**4**)	11.2 ± 0.01	−6.2 ± 0.3	−0.5 ± 0.3	3.6 ± 0.08
BPAM97 (**2**)[d]	5.6 ± 0.9	−4.9 ± 0.4	−2.3 ± 0.4	3.0 ± 0.2

[a]Sites per LBD dimer.
[b]Standard deviation.
[c]Values from (12).
[d]Values from (7).

Fig. 7. Generally, it appears that the binding of BPAMs with an electronegative atom or substituent in the 7-position (BPAM25 (**11**), **2**, **3**, **4**, and **5**) is mainly driven by enthalpy, whereas an electronegative atom or substituent in the 5- or 6-position (BPAM408 (**13**) and BPAM429 (**15**)) changes the profile so that binding is mainly entropy driven. Introduction of an electronegative atom or substituent in the 8-position (BPAM37 (**12**) and BPAM442 (**16**)) seems to render the binding equally enthalpy and entropy driven. Interestingly, compound IDRA21 (**1**) containing a different substitution pattern in the thiadiazine scaffold is mainly driven by entropy. This observation is consistent with a scaffold reorientation of **1** compared to the BPAMs, leading to a location of the chlorine atom of **1** in the direction of the 6-position of BPAMs (Fig. 5 *C*). However, Ser-497 is also likely to be less fixed with a lesser loss of disorder.

A comparison of the binding mode of **5** to that of **3** shows that the favorable enthalpy most likely arises from the hydrogen bond between the 7-hydroxyl group and Ser-497. On the other hand, differences in binding affinities of **4** and **5** versus those of their fluorinated counterparts **2** and **3** are marginal. This is due to less favorable binding entropies for **4** and **5**. Two major terms are important for the entropy of binding: 1) change in solvent entropy arising from desolvation of the modulator and receptor binding site upon binding and 2) change in conformational degrees of freedom in the modulator and receptor upon binding. The change in desolvation entropy will be most favorable if surfaces buried upon binding are predominantly hydrophobic. Because **5** was found to be ~eightfold more soluble in water compared to **3** (2.4 ± 0.1 mM vs. 0.29 ± 0.04 mM at room temperature (24)), from a desolvation point of view it is presumably more favorable to bury the 7-fluorinated compound **3** compared to **5** containing a 7-hydroxyl group. A similar conclusion can be deduced with **2** and **4** based on their respective water solubility at room temperature (**4**: 2.90 ± 0.04 mM; **2**: 1.65 ± 0.04 mM; data not shown).

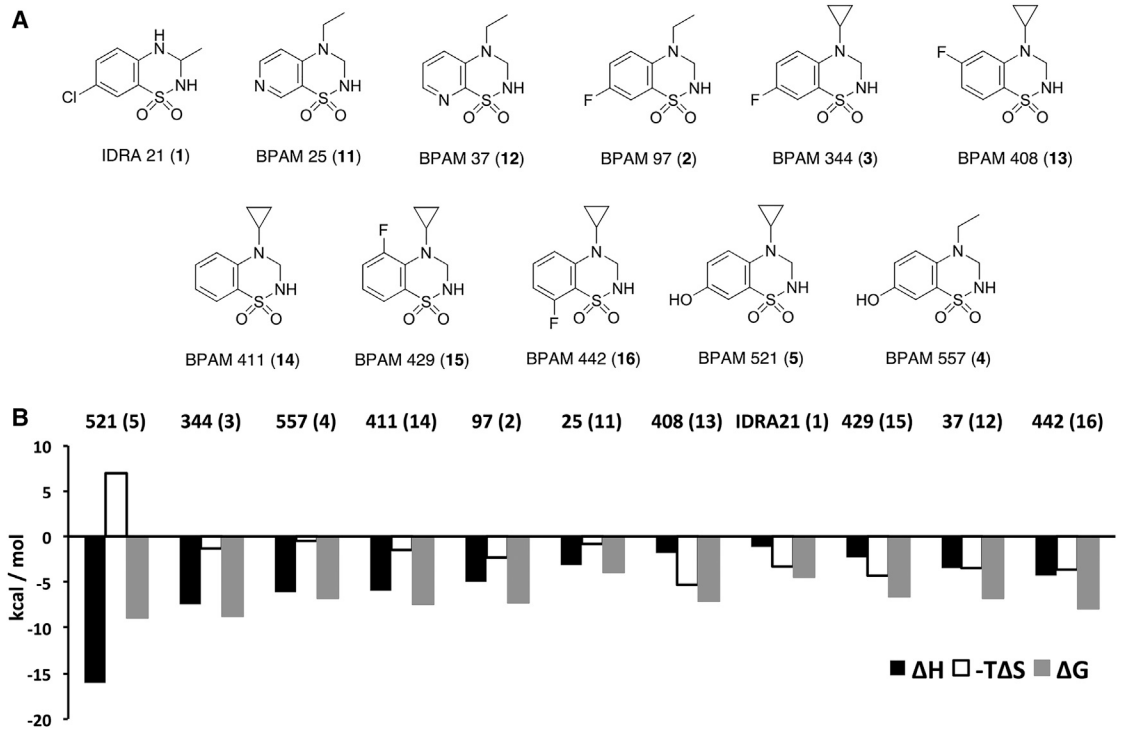

FIGURE 7 Thermodynamics of binding of BPAM modulators measured by ITC. (*A*) Structures of IDRA21 (**1**) and 10 BPAMs investigated to date. (*B*) Enthalpy, entropy, and free energy contributions to binding are shown as black, white, and gray columns, respectively. Listed from left are compounds for which binding is mainly driven by enthalpy: BPAM521 (**5**) (this study), BPAM344 (**3**) (12), BPAM557 (**4**) (this study), BPAM411 (**14**) (27), BPAM97 (**2**) (7), and BPAM25 (**11**) (13). The compounds are listed according to the difference between ΔH and –TΔS, with the largest difference to the left and smallest to the right, and then compounds mainly driven by entropy are listed: BPAM408 (**13**) (27), IDRA21 (**1**) (7), and BPAM429 (**15**) (27). Finally, compounds equally driven by enthalpy and entropy are listed: BPAM37 (**12**) (13) and BPAM442 (**16**) (27).

Moreover, the 4-ethyl-substituted compounds (**2** and **4**) are more soluble than their 4-cyclopropyl counterparts (**3** and **5**). We calculated SM8 solvation energies (22) for compounds **2**–**5**, showing that the estimated solvation energy of **4** and **5** (−18.1 and −18.4 kcal/mol, respectively) is more favorable than for **2** and **3** (−14.3 and −14.6 kcal/mol, respectively). The influence of cyclopropyl (**3** and **5**) versus ethyl (**2** and **4**) seems to be negligible based on the estimated solvation energies. Therefore, the observed difference in experimental water solubility between ethyl and cyclopropyl (**2** vs. **3** and **4** vs. **5**) seems not to be reflected in the SM8 solvation energies. However, the uncertainty of 0.5–0.8 kcal/mol on the SM8 solvation energies should be kept in mind. Another likely contribution to the less favorable binding entropy with the exchange of the 7-fluorine with a hydroxyl group is introduction of an entropy penalty for the higher ordering of the Ser-497 side chain and the modulator hydroxyl group in the **4** and **5** complexes compared to the structures with **2** and **3**. Therefore, the unfavorable entropy might be partly due to desolvation of more soluble compounds **4** and **5** and partly to conformational restriction of Ser-497 by the added hydroxyl group of compound **5** and possibly also **4**. The presence of the cyclopropyl group on **3** has previously been shown to increase favorable enthalpy and affinity, over the ethyl substituted compound **2** due to pi-interactions of the cyclopropyl group with Met-496 (12). This is corroborated by this study in comparing the thermodynamic data obtained for **5** with those of **4**. Interestingly, comparing **2** with **4** we observe a lesser gain in favorable enthalpy and lesser loss of favorable entropy from the exchange of F with OH than when comparing **3** with **5**. Intuitively, one would have expected additivity of the substituents. However, other examples on nonadditivity of substituents have previously been reported, e.g., see (25).

In conclusion, we have reported the synthesis of two new positive allosteric modulators of AMPA receptors (**4** and **5**) that are 7-hydroxyl substituted analogs of the previously reported compounds **2** and **3**, respectively. We have investigated the binding mode of **5** using x-ray crystallography and shown that this substitution enables a hydrogen bond to the side chain of Ser-497. We suggest that the conformation of Ser-497 in the GluA2 LBD complex with **5** is due to lack of repulsion from the modulator and that this favors an interaction between Ser-497 and the hydroxyl group of **5**. In addition, we investigated the effects of the substitution on the affinities and thermodynamics of binding using ITC. This revealed that compared to their fluorinated counterparts **2** and **3**, the new positive allosteric modulators **4** and **5** show a favorable decrease in binding enthalpy but also equally nonfavorable binding entropy, leaving the affinity and potency of the compounds essentially unchanged. This more favorable binding enthalpy can be explained by the formation of a hydrogen bond between **5** and Ser-497 in GluA2. The decrease in the favorable binding entropy is most likely caused by an entropy penalty arising from desolvation effects and conformational constraints imposed on Ser-497 and possibly also on the hydroxyl group of the modulator.

ACCESSION NUMBERS

The accession number for the structure coordinates and corresponding structure factor file of GluA2 LBD-L483Y-N754S with BPAM521 (**5**) reported in this paper is Protein Data Bank: 5ELV.

AUTHOR CONTRIBUTIONS

C.K., P.F., D.S.P., J.P., L.O., E.G., B.P., and J.S.K. designed research; C.K., P.F., D.S.P., L.J., and E.G. performed research; C.K., P.F., D.S.P., L.J., J.P., L.O., K.F., E.G., B.P., and J.S.K. analyzed data. C.K., P.F., D.S.P., B.P., and J.S.K. wrote the first draft of the article. B.P. and J.S.K. equally supervised the work.

ACKNOWLEDGMENTS

Heidi Peterson is thanked for help with expression and purification of GluA2 LBD-L483Y-N754S and MAX-Lab, Lund, Sweden is thanked for providing beamtime.

We thank the Danish Council for Independent Research | Medical Sciences (to C.K. and J.S.K.), the Lundbeck Foundation (to J.P., L.O., and J.S.K.), GluTarget (to C.K., L.J., K.F., and J.S.K.), and Danscatt (to C.K., L.J., K.F., and J.S.K.) for financial support.

REFERENCES

1. Traynelis, S. F., L. P. Wollmuth, …, R. Dingledine. 2010. Glutamate receptor ion channels: structure, regulation, and function. *Pharmacol. Rev.* 62:405–496.
2. Sobolevsky, A. I., M. P. Rosconi, and E. Gouaux. 2009. X-ray structure, symmetry and mechanism of an AMPA-subtype glutamate receptor. *Nature.* 462:745–756.
3. Armstrong, N., and E. Gouaux. 2000. Mechanisms for activation and antagonism of an AMPA-sensitive glutamate receptor: crystal structures of the GluR2 ligand binding core. *Neuron.* 28:165–181.
4. Sun, Y., R. Olson, …, E. Gouaux. 2002. Mechanism of glutamate receptor desensitization. *Nature.* 417:245–253.
5. Jin, R., S. Clark, …, K. M. Partin. 2005. Mechanism of positive allosteric modulators acting on AMPA receptors. *J. Neurosci.* 25:9027–9036.
6. Stern-Bach, Y., S. Russo, …, C. Rosenmund. 1998. A point mutation in the glutamate binding site blocks desensitization of AMPA receptors. *Neuron.* 21:907–918.
7. Krintel, C., K. Frydenvang, …, J. S. Kastrup. 2012. Thermodynamics and structural analysis of positive allosteric modulation of the ionotropic glutamate receptor GluA2. *Biochem. J.* 441:173–178.
8. Francotte, P., Pd. Tullio, …, B. Pirotte. 2007. Design, synthesis, and pharmacology of novel 7-substituted 3,4-dihydro-2H-1,2,4-benzothiadiazine 1,1-dioxides as positive allosteric modulators of AMPA receptors. *J. Med. Chem.* 50:3153–3157.
9. Yamada, K. A., and S. M. Rothman. 1992. Diazoxide blocks glutamate desensitization and prolongs excitatory postsynaptic currents in rat hippocampal neurons. *J. Physiol.* 458:409–423.
10. Yamada, K. A., and C. M. Tang. 1993. Benzothiadiazides inhibit rapid glutamate receptor desensitization and enhance glutamatergic synaptic currents. *J. Neurosci.* 13:3904–3915.

11. Ptak, C. P., A. H. Ahmed, and R. E. Oswald. 2009. Probing the allosteric modulator binding site of GluR2 with thiazide derivatives. *Biochemistry.* 48:8594–8602.
12. Nørholm, A. B., P. Francotte, …, J. S. Kastrup. 2013. Synthesis, pharmacological and structural characterization, and thermodynamic aspects of GluA2-positive allosteric modulators with a 3,4-dihydro-2H-1,2,4-benzothiadiazine 1,1-dioxide scaffold. *J. Med. Chem.* 56:8736–8745.
13. Francotte, P., A. B. Nørholm, …, B. Pirotte. 2014. Positive allosteric modulators of 2-amino-3-(3-hydroxy-5-methylisoxazol-4-yl)propionic acid receptors belonging to 4-cyclopropyl-3,4-dihydro-2h-1,2,4-pyridothiadiazine dioxides and diversely chloro-substituted 4-cyclopropyl-3,4-dihydro-2H-1,2,4-benzothiadiazine 1,1-dioxides. *J. Med. Chem.* 57:9539–9553.
14. Girard, Y., J. G. Atkinson, and J. Rokach. 1979. A new synthesis of 1,2,4-benzothiadiazines and a selective preparation of o-aminobenzenesulfonamides. *J. Chem. Soc., Perkin Trans. 1*. 1043–1047.
15. Ursby, T., J. Unge, …, M. M. Thunnissen. 2013. The macromolecular crystallography beamline I911–3 at the MAX IV laboratory. *J. Synchrotron Radiat.* 20:648–653.
16. Battye, T. G., L. Kontogiannis, …, A. G. Leslie. 2011. iMOSFLM: a new graphical interface for diffraction-image processing with MOSFLM. *Acta Crystallogr. D Biol. Crystallogr.* 67:271–281.
17. Collaborative Computational Project, Number 4. 1994. The CCP4 suite: programs for protein crystallography. *Acta Crystallogr. D Biol. Crystallogr.* 50:760–763.
18. McCoy, A. J., R. W. Grosse-Kunstleve, …, R. J. Read. 2007. Phaser crystallographic software. *J. Appl. Cryst.* 40:658–674.
19. Emsley, P., B. Lohkamp, …, K. Cowtan. 2010. Features and development of Coot. *Acta Crystallogr. D Biol. Crystallogr.* 66:486–501.
20. Adams, P. D., P. V. Afonine, …, P. H. Zwart. 2010. PHENIX: a comprehensive Python-based system for macromolecular structure solution. *Acta Crystallogr. Sect. D: Biol. Crystallogr.* 66:213–221.
21. Hayward, S., and H. J. Berendsen. 1998. Systematic analysis of domain motions in proteins from conformational change: new results on citrate synthase and T4 lysozyme. *Proteins.* 30:144–154.
22. Marenich, A. V., R. M. Olson, …, D. G. Truhlar. 2007. Self-consistent reaction field model for aqueous and nonaqueous solutions based on accurate polarized partial charges. *J. Chem. Theory Comput.* 3:2011–2033.
23. Ptak, C. P., C. L. Hsieh, …, R. E. Oswald. 2014. Role of stoichiometry in the dimer-stabilizing effect of AMPA receptor allosteric modulators. *ACS Chem. Biol.* 9:128–133.
24. Larsen, A. P., P. Francotte, …, J. S. Kastrup. 2016. Synthesis and pharmacology of mono-, di- and trialkyl-substituted 7-chloro-3,4-dihydro-2H–1,2,4-benzothiadiazine 1,1-dioxides combined with X-ray structure analysis to understand the unexpected structure-activity relationship at AMPA receptors. *ACS Chem. Neurosci.* 7:378–390.
25. Biela, A., M. Betz, …, G. Klebe. 2012. Water makes the difference: rearrangement of water solvation layer triggers non-additivity of functional group contributions in protein-ligand binding. *ChemMedChem.* 7:1423–1434.
26. Laskowski, R. A., M. W. MacArthur, …, J. M. Thornton. 1993. PROCHECK: a program to check the stereochemical quality of protein structures. *J. Appl. Cryst.* 26:283–291.
27. Nørholm, A. B., P. Francotte, …, C. Oostenbrink. 2014. Thermodynamic characterization of new positive allosteric modulators binding to the glutamate receptor A2 ligand-binding domain: combining experimental and computational methods unravels differences in driving forces. *J. Chem. Inf. Model.* 54:3404–3416.